Chemical Engineering Journal 269 (2015) 135–147

Contents lists available at ScienceDirect

Chemical Engineering Journal

journal homepage: www.elsevier.com/locate/cej

Utilizing transient breakthroughs for evaluating the potential of Kureha carbon for CO_2 capture

Hui Yu [a], Xue Wang [a], Chunhui Xu [a], De-Li Chen [a], Weidong Zhu [a,*], Rajamani Krishna [b,*]

[a] Key Laboratory of the Ministry of Education for Advanced Catalysis Materials, Institute of Physical Chemistry, Zhejiang Normal University, 321004 Jinhua, PR China
[b] Van't Hoff Institute for Molecular Science, University of Amsterdam, Science Park 904, 1098 XH Amsterdam, The Netherlands

HIGHLIGHTS

- Highly selective adsorption of CO_2 over N_2 and CH_4 on Kureha carbon.
- Simulation methodology for transient breakthroughs in fixed-bed adsorbers.
- IAST calculations satisfactorily predict the separation performance.
- Kureha carbon is potential for separating CO_2/N_2 and CO_2/CH_4 mixtures.

GRAPHICAL ABSTRACT

The commercial Kureha carbon, a purely microporous material, is a potential adsorbent for the selective separations of CO_2/N_2 and CO_2/CH_4 mixtures.

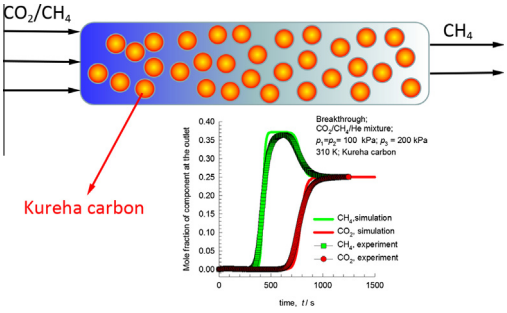

ARTICLE INFO

Article history:
Received 20 November 2014
Received in revised form 22 January 2015
Accepted 24 January 2015
Available online 2 February 2015

Keywords:
Activated carbon
CO_2 separation
Transient breakthrough
Adsorption
Microporous material

ABSTRACT

The commercial Kureha carbon was used as adsorbent for the selective adsorption of CO_2 over N_2 and CH_4. The single-component isotherms are reported at pressures up to 2500 kPa and at 298, 310, and 323 K. The Langmuir–Freundlich model appropriately describes the adsorption equilibrium data over the whole range of conditions. The extracted isosteric heat of adsorption of CO_2 on Kureha carbon is significantly lower than those on zeolite NaX and some metal–organic frameworks that are considered to be promising candidates for CO_2 capture; this implies that the cost of regeneration with Kureha carbon can be potentially lower. The selective separations of two mixtures CO_2/CH_4 and CO_2/N_2 on Kureha carbon were experimentally investigated by a breakthrough-column technique. The simulations of transient breakthroughs for CO_2/CH_4 and CO_2/N_2 mixtures agree reasonably well with the experimental data. The breakthrough simulations also indicate that the separation performance is not significantly influenced by intra-particle diffusion resistances. Furthermore, the ideal adsorbed solution theory calculations are found to satisfactorily predict the experimentally observed separation performance. The investigations lead to the conclusion that Kureha carbon has a significant potential for CO_2 uptake from flue gas mixtures.

1. Introduction

One of the primary issues nowadays is the discussion, observation, and investigation of global climate change and the need to reduce greenhouse gas emissions. The sharply rising level

* Corresponding authors. Tel.: +86 579 82282932 (W. Zhu).
E-mail addresses: weidongzhu@zjnu.cn (W. Zhu), r.krishna@contact.uva.nl (R. Krishna).

http://dx.doi.org/10.1016/j.cej.2015.01.091
1385-8947/

Nomenclature

A	cross-sectional area of the breakthrough column (m^2)
B	adsorption equilibrium constant in the Langmuir–Freundlich model (Pa^{-v})
b_0	adsorption equilibrium constant in the Langmuir–Freundlich model (Pa^{-v})
c_t	total molar concentration of the gas mixture (mol m^{-3})
E	energy parameter in the Langmuir–Freundlich model (J mol^{-1})
L	length of the packed bed adsorber (m)
m_{ads}	mass of the adsorbent particles packed into the breakthrough column (kg)
p	pressure (Pa)
p_i	partial pressure of species i in the mixture (Pa)
p_t	total system pressure (Pa)
q	adsorbed amount (mol kg^{-1}) or (mol m^{-3})
Q_{He}	volumetric flow rate of the inert gas He (m^3 s^{-1})
q_i	component molar loading of species i (mol kg^{-1})
q_{sat}	adsorption saturation capacity (mol kg^{-1})
Q_{st}	isosteric heat of adsorption (J mol^{-1})
Q_{st}^0	isosteric heat of adsorption at zero loading (J mol^{-1})
R	universal gas law constant (8.314 J mol^{-1} K^{-1})
S_{ads}	adsorption selectivity, dimensionless
S_{BET}	BET specific surface area of adsorbent (m^2 kg^{-1})
t	time (s)
T	temperature (K)
t_{ss}	total period of time till the steady-state is reached (s)
V_{ads}	volume of the adsorbent packed into the breakthrough column (m^3)
V_{tot}	total pore volume of adsorbent (m^3 kg^{-1})
y_i	mole fraction of component i in the bulk gas phase, dimensionless

Greek letters

v	exponent in the dual-Langmuir–Freundlich isotherm, dimensionless
ρ	particle density of adsorbent (kg m^{-3})
ρ_{grain}	grain density of adsorbent (kg m^{-3})

of atmospheric CO_2, being one of the predominant greenhouse gases, resulting from anthropogenic emissions, is one of the greatest environmental concerns facing our civilization today. These emissions, which stem predominantly from the combustion of coal, oil, and natural gas (ca. 80% of CO_2 emissions worldwide) [1], are projected to continuously increase in the future due to economic growth and industrial development, particularly in developing nations [2]. One option for reducing these CO_2 emissions has been termed carbon capture and sequestration (CCS), in which the most costly step is the CO_2 separation one [3]. In addition, the separation of CO_2 from CH_4 is also an important process in natural gas upgrading.

Amine scrubbing is an extensively investigated method of capturing CO_2 from coal-fired power plant exhaust gas (flue gas); however, the process is energy-intensive [4] and requires waste treatment for amine degradation products and side products [5]. These factors necessitate a continuous search for more efficient and environmentally friendly ways to capture CO_2 from various gas streams. A potentially viable alternative is a system that uses a porous material to selectively adsorb CO_2 from various gas streams. This could be advantageous because the separation and recovery of CO_2 can be performed under relatively mild conditions when compared with amine scrubbing systems.

Combining the high affinity of amines and the advantages of using porous solid adsorbents holds promise for the development of new materials that exhibit appropriate properties for CO_2 capture applications. Indeed, amino-functionalized mesoporous silicas, especially those synthesized from parent mesoporous SBA-15 materials, show some promising properties, such as the reversible formation of ammonium carbamates and/or carbonates during CO_2 adsorption and their uniform, large pore, and high surface area, for CO_2 capture and separation [6,7]. In addition, the presence of moisture can enhance the adsorption capacity of CO_2 on these amino-functionalized adsorbents [7]. However, these amino-functionalized adsorbents are often regenerated at high temperatures due to the high affinity of the amino groups to the adsorbed CO_2 molecules, resulting in a high energy input for their regeneration.

Zeolites have been studied especially in the context of the upgrading of natural gas and CO_2 capture from post-combustion flue gas. For example, zeolite 13X, which has a relatively high surface area and micropore volume, has been shown to display promising capacities for CO_2 at room temperature (3.73 mol kg^{-1} at 80 kPa and 298 K) [8]. The large variety of zeolite structures that have been reported to date presents an opportunity for the study of the effects of composition or certain structural or chemical features on the adsorption performance [9]. For example, it has been observed that the Si/Al ratio of zeolites can have a significant impact on CO_2 adsorption, which in turn has crucial implications toward the adsorption selectivity and regeneration costs associated with the capture process [10]. In comparison with post-combustion CO_2 capture employing amine solutions discussed above, small-scale pilot plants using zeolites have demonstrated more rapid adsorption of CO_2 and lower energy penalty for the process [11]. However, many of the zeolites with low Si/Al ratios studied to date become readily saturated with the water vapor present in the flue gas stream, because these zeolites are hydrophilic in nature and their CO_2 adsorption capacities are consequently reduced over time [12,13]. Furthermore, the large adsorption enthalpy of CO_2 on zeolite 13X leads to relatively high CO_2 desorption temperatures (ca. 400 K) [14]. Increasing the Si/Al ratios of zeolites can weaken the affinity of the zeolite pore surfaces toward CO_2 and reduce the effects of the presence of moisture on CO_2 adsorption. For example, pure silica zeolites silicalite-1 and DD3R can selectively adsorb CO_2 over CH_4 and N_2 but these hydrophobic zeolites have low adsorption capacities for CO_2 [15,16].

Metal–organic frameworks (MOFs) are a class of porous crystalline hybrid materials with high tunability, derived from the almost limitless choice of inorganic clusters (connectors) linked together by organic linkers. By varying the organic linker, the pore size and structure of MOFs can be tailored, while functional groups can be introduced at the linker or connector to create specific adsorption sites. Recently, MOFs have been extensively investigated for CO_2 capture and their results have been addressed in three review articles [3,17,18]. Many MOFs have high CO_2 adsorption capacities and selectivities over N_2 and CH_4 [19–25]. However, the presence of moisture can significantly reduce the adsorption capacities of CO_2 on most MOFs [26,27]. In addition, the cost and scale-up in the preparation of MOFs have probably limited their development for practical applications, although efforts have been made [17].

Activated carbons have also attracted much interest as CO_2 adsorbents. These materials are amorphous porous forms of carbon

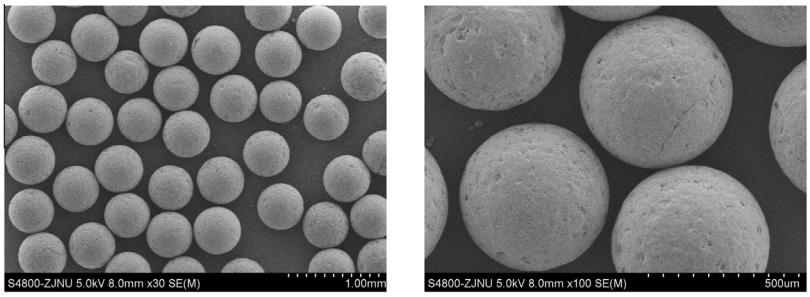

Fig. 1. SEM images of the Kureha carbon particles used in this study.

Table 1
Textural properties of Kureha carbon and the benchmark activated carbon Maxsorb.

Adsorbent	S_{BET}, $m^2\ g^{-1}$		V_{tot} ($cm^3\ g^{-1}$)	ρ_{grain} ($kg\ m^{-3}$)	ρ ($kg\ m^{-3}$)
	Total	>2 nm[a]			
Kureha carbon	1300	0	0.56	1860	991
Maxsorb	3250[b]	1070[c]	1.79[b]		290[b]

[a] BET surface area at pore sizes larger than 2 nm.
[b] Data from Ref. [40].
[c] Data from Ref. [41].

Table 2
Estimated parameter values for the combined fitting of the adsorption isotherm data of CO_2, CH_4, and N_2 on Kureha carbon by the Langmuir–Freundlich model and the derived isosteric heat of adsorption at zero loading.

Adsorbate	q_{sat} ($mol\ kg^{-1}$)	b_0 ($Pa^{-\nu}$)	E ($kJ\ mol^{-1}$)	ν	Q_{st}^0 ($kJ\ mol^{-1}$)
CO_2	15.3	1.68×10^{-8}	16.9	0.82	20.6
CH_4	8.5	2.16×10^{-8}	13.6	0.89	15.3
N_2	5.4	1.01×10^{-8}	10.4	1	10.4

that can be prepared by pyrolysis of various carbon-containing resins, fly ash, or biomass [28]. The main advantage of activated carbons over zeolites and/or MOFs for CO_2 capture is that their hydrophobic nature results in a reduced effect of the presence of moisture, and they consequently do not suffer from decomposition or decreased capacities under hydrated conditions [29]. Moreover, due to the lower heat of adsorption for CO_2, activated carbons demand lower regeneration energies as compared with zeolites [29].

Activated carbons have many different brands to choose from and their properties depend on the starting material and the manufacturing process. In fact, a lot of adsorption isotherm data for different adsorbates on various activated carbons have been reported in the open literature. The accumulation of a data bank can be found in a handbook by Valenzuela and Myers [30]. Particularly, Martin et al. [31] recently reported the isotherm data of CO_2 on 23 types of activated carbons with a large variety of porous characteristics at 298 K and at 100 and 2000 kPa, respectively, indicating that the process of CO_2 capture at the lower pressure involves exclusively the smaller micropores of the activated carbons and the maxima CO_2 retention capacities can only be found for the adsorbents with a high micropore volume coming from pores below 0.6 nm while the CO_2 uptake at the higher pressure occurs by filling of the entire microporosity, followed by filling of the mesopores and macropores if available. In addition, the presence of supermicropores may enhance the kinetics of the CO_2 capture process by providing wider transport paths into the smaller pores [31]. Similarly, other researchers [32–35] also pointed out that CO_2 adsorption on activated carbons at low pressures would take place via a volume-filling mechanism and the micropore size limits for the volume-filling could be below 0.8 nm. In terms of porous characteristics, therefore, the commercial Kureha carbon [36–39], a purely microporous material with pore-size distribution centered at 0.6 and 1.1 nm, respectively [36], could be a promising adsorbent for CO_2 capture. The aims of the present study are twofold. The first objective is to demonstrate the potential of Kureha carbon for the separations of CO_2/N_2 and CO_2/CH_4 mixtures. Therefore, the single-component isotherms of CO_2, N_2, and CH_4 on Kureha carbon are measured and then described by a proper isotherm model. The transient breakthroughs are experimentally determined for the two mixtures CO_2/N_2 and CO_2/CH_4 in a fixed bed packed with spherical Kureha carbon beads with uniform shape and size. The second objective is to verify the adopted modeling procedure by the comparisons of the simulated and experimental breakthroughs.

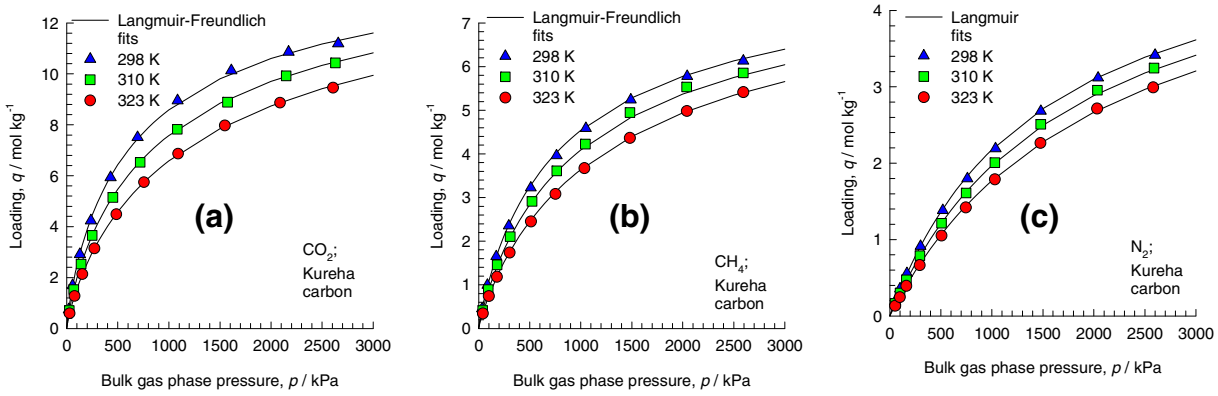

Fig. 2. Comparison of the pure component isotherm data of (a) CO_2, (b) CH_4, and (c) N_2 on Kureha carbon with the fitted Langmuir–Freundlich isotherms (shown by continuous solid lines) at 298, 310, and 323 K.

Table 3
Comparison of the pure component isotherm data of CO_2, CH_4, and N_2 on Kureha carbon with those on the benchmark activated carbon Maxsorb at low and high pressures of 100 and 2000 kPa, respectively, and at 298 K.

Adsorbate	q, mol kg^{-1}		q, mmol cm^{-3}[a]	
	100 kPa	2000 kPa	100 kPa	2000 kPa
Kureha carbon				
CO_2	2.49	10.6	2.47	10.5
CH_4	1.09	5.78	1.08	5.73
N_2	0.340	3.10	0.337	3.07
Maxsorb[b]				
CO_2	2.19	19.5	0.635	5.66
CH_4	1.13	9.31	0.328	2.70
N_2	0.322	3.80	0.093	1.10

[a] Volumetric adsorption capacity, calculated from the gravimetric adsorption capacity multiplied by the particle density of adsorbent shown in Table 1.
[b] Adsorption isotherm data of CO_2 and CH_4 at 298 K from Ref. [40] while the adsorption isotherm data of N_2 at 300 K from Ref. [44].

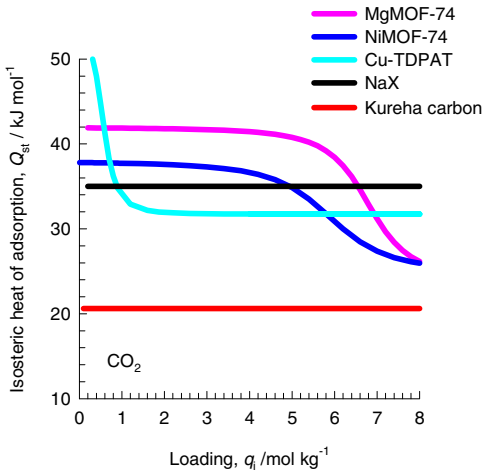

Fig. 3. Comparison of the isosteric heat of adsorption for CO_2 on Kureha carbon with the data from the literature on NaX [45], MgMOF-74 [45], Cu-TDPAT [46] and NiMOF-74 [47,48].

2. Experimental

2.1. Adsorbent

The commercial sample, spherical bead activated carbon, was supplied by Kureha Chemical Industry. This activated carbon is referred to as Kureha carbon. The morphology and particle size of Kureha carbon were examined with scanning electron microscopy (SEM). The SEM images were obtained using a Hitachi S-4800 instrument operating at 5.0 kV. Kureha carbon particles in this study had an average diameter of 0.52 mm, as shown in Fig. 1.

The textural properties of Kureha carbon were evaluated by N_2 adsorption at 77 K using a Micromeritics ASAP 2020 instrument. The sample was outgassed under vacuum at 423 K for 10 h, prior to the adsorption measurement. The specific surface area of the adsorbent was calculated using the multiple-point Brunauer–Emmett–Teller (BET) method in a relative pressure range of p/p_0 = 0.05–0.20, and the total pore volume was determined at a relative pressure of 0.95. The pore size distribution was evaluated in terms of the density functional theory (DFT) simulation using the isotherm data of N_2 adsorption at 77 K and relative pressures up to 0.20. Only micropores contribute to the total pore volume and the surface area. This was further confirmed by mercury intrusion porosimetry; no significant additional porosity was observed in the pore size range from 2 to 100 nm. A plot of differential pore volume as a function of pore width is reported elsewhere [36], in which there are two maxima at 0.6 and 1.1 nm, respectively. The grain density (ρ_{grain}) of Kureha carbon was measured by He pycnometry (Micromeritics AccuPyc II 1340), which was used to calculate its particle density (ρ). The textural properties of the adsorbent are summarized in Table 1.

2.2. Adsorption equilibrium measurements

The single-component adsorption isotherms of CO_2, CH_4, and N_2 on Kureha carbon were measured by a Particulate Systems HPVA-200 instrument. The sample cell was loaded with 0.827 g of Kureha carbon particles. The adsorbent was outgassed under vacuum at 573 K for 12 h in order to remove any adsorbed impurities, prior to the adsorption measurements. The obtained dry sample mass was used in the calculation of isotherm data. The adsorption runs were carried out at pressures up to 2,500 kPa and three different temperatures (298, 310, and 323 K). A circulating water bath was used to control the temperatures within ±0.1 K.

2.3. Transient breakthrough experiments

The breakthrough-column setup consists of three sections: a gas mixing and flow control section, a breakthrough column, and an analysis section. The flow-sheet diagram and detailed description of the breakthrough setup are given elsewhere [42,43]. The breakthrough column was installed inside the ceramic oven, which was located inside the convection oven. The external diameter of the column was 6.35 mm with a length of

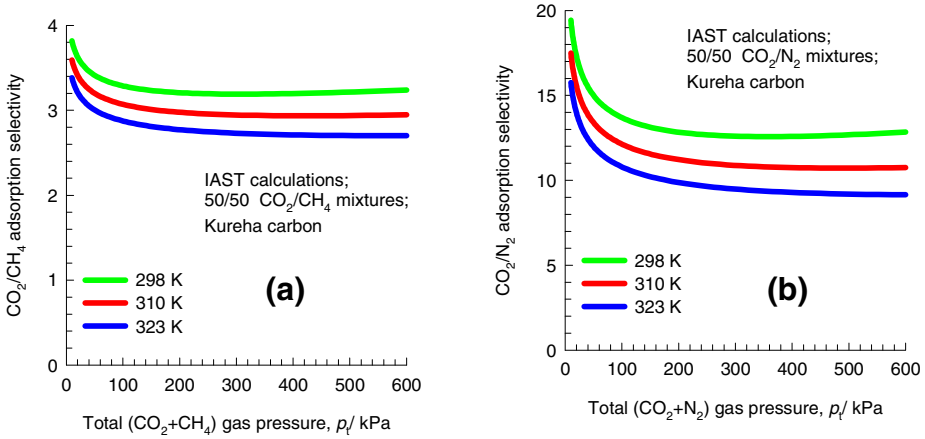

Fig. 4. Adsorption selectivity as a function of total gas-phase pressure calculated by IAST for equimolar binary (a) CO_2/CH_4 and (b) CO_2/N_2 gas mixtures on Kureha carbon.

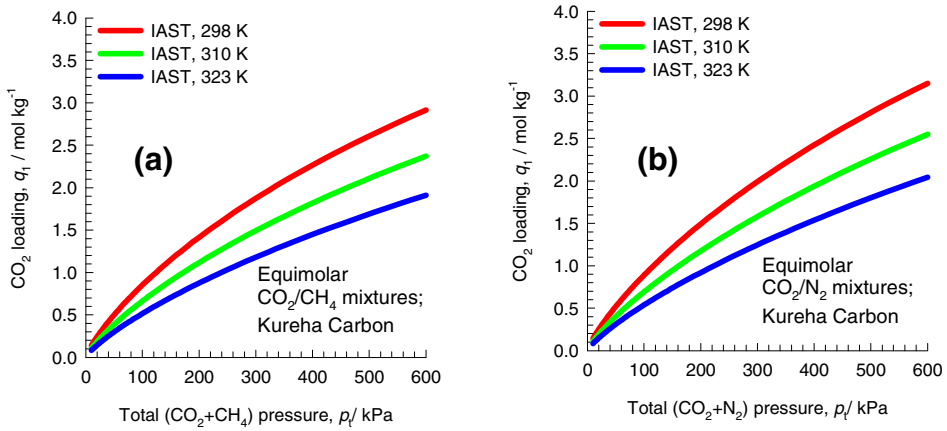

Fig. 5. Uptake capacity of CO_2 from equimolar binary (a) CO_2/CH_4 and (b) CO_2/N_2 gas mixtures on Kureha carbon as a function of total gas phase pressure calculated by IAST.

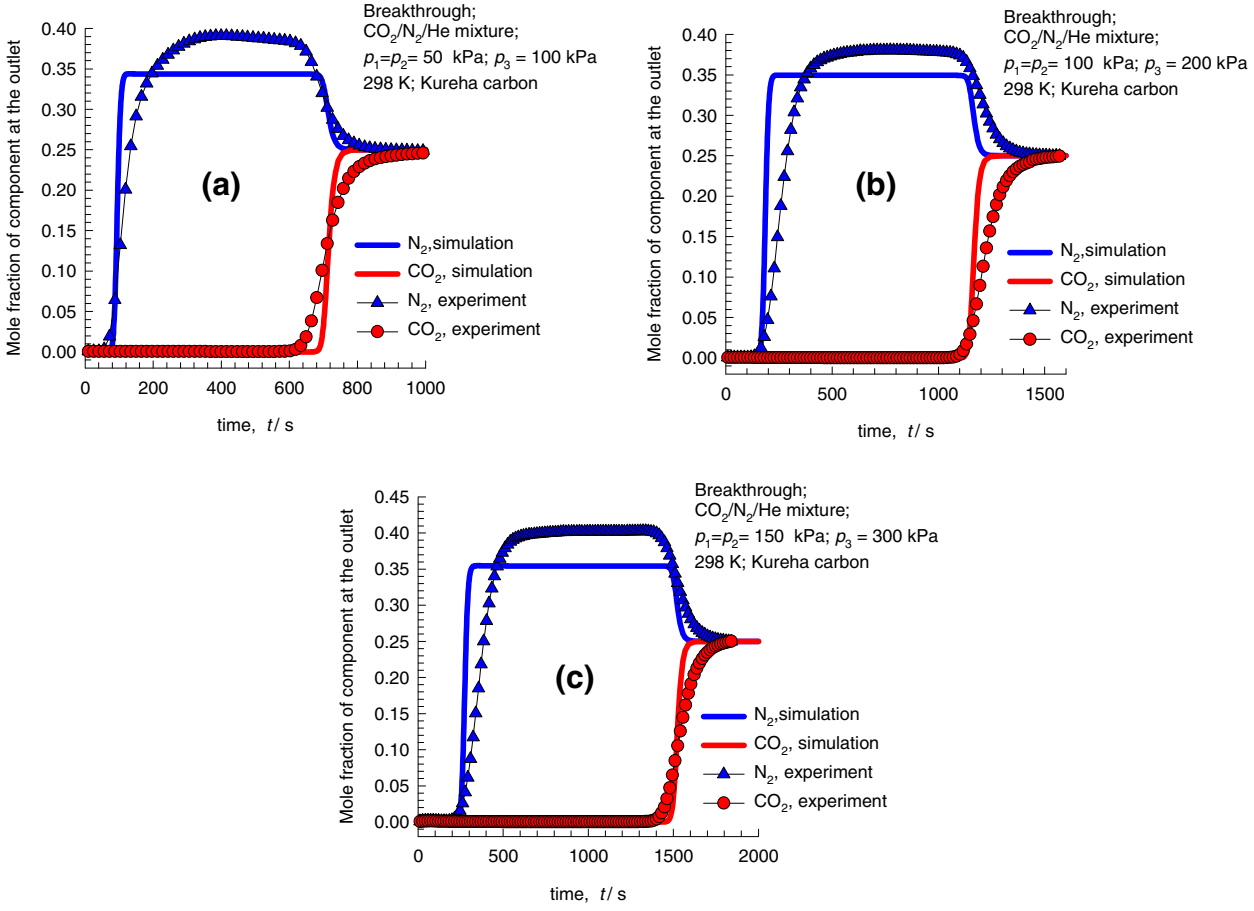

Fig. 6. Comparison of the experimental breakthroughs for $CO_2(1)/N_2(2)/He(3)$ with the corresponding breakthrough simulations at 298 K. (a) $p_1 = p_2 = 50$ kPa and $p_3 = 100$ kPa, (b) $p_1 = p_2 = 100$ kPa and $p_3 = 200$ kPa, and (c) $p_1 = p_2 = 150$ kPa and $p_3 = 300$ kPa. The continuous solid lines are the simulations assuming negligible diffusional limitations and invoking Eq. (A9). A video animation of the transient breakthrough at 298 K and a total pressure of 200 kPa is available as Supplementary material.

10 cm, and the inner diameter was 4.65 mm. A 0.76 g amount of Kureha carbon particles was packed into the column. The quartz wool was placed at the top and bottom of the column. Prior to the breakthrough experiments, the adsorbent was outgassed overnight at 473 K with a He flow rate of 20 ml (STP) min^{-1} (STP: standard temperature and pressure). The breakthrough curves were then measured by switching the He flow to a flow containing CO_2 and CH_4 (or CO_2 and N_2) in He (used as a balance) with a CO_2:CH_4:He (or CO_2:N_2:He) mole composition of 1:1:2 at a total flow rate of 8 ml (STP) min^{-1}. The breakthrough experiments were performed at three different temperatures (298, 310, and 323 K) and the total pressures of the ternary gas mixtures were maintained at 200, 400, and 600 kPa, respectively, for all three breakthrough experiments at each temperature. The partial pressures of CO_2 and CH_4 (or CO_2 and N_2) were varied from 50 to 100 and 150 kPa at the inlet of the column by altering the total pressures from 200 to 400 and 600 kPa, respectively. The mass spectrometer (Pfeiffer Vacuum OmniStar GSD 320) in the analysis section was used to monitor the component concentrations continuously. After each breakthrough experiment, the

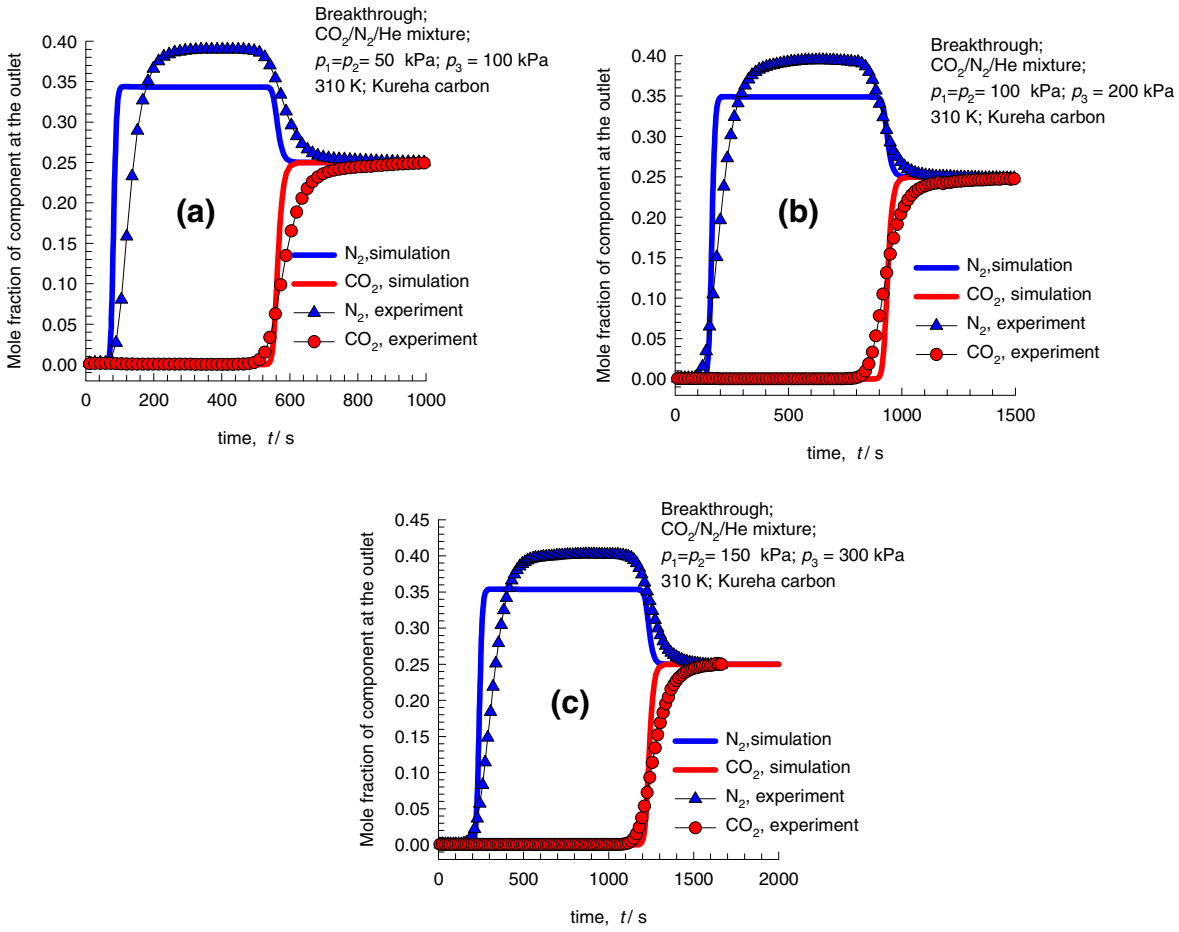

Fig. 7. Comparison of the experimental breakthroughs for $CO_2(1)/N_2(2)/He(3)$ with the corresponding breakthrough simulations at 310 K. (a) $p_1 = p_2 = 50$ kPa and $p_3 = 100$ kPa, (b) $p_1 = p_2 = 100$ kPa and $p_3 = 200$ kPa, and (c) $p_1 = p_2 = 150$ kPa and $p_3 = 300$ kPa. The continuous solid lines are the simulations assuming negligible diffusional limitations and invoking Eq. (A9).

column was flushed with flowing He at 20 ml (STP) min^{-1} for 6 h at the measurement temperature.

The used gases had the following purities: CO_2 (99.999%), CH_4 (99.99%), N_2 (99.999%), and He (99.999%).

3. Results and discussion

3.1. Adsorption isotherms

The adsorption isotherms of CO_2, CH_4, and N_2 on Kureha carbon were measured at 298, 310, and 323 K, as shown in Fig. 2. From a fundamental point of view, the experimental data should be correlated with an analytical expression that includes the temperature dependency. Various empirical methods have been proposed to fit isotherm data in adsorption science. In many cases, however, it may not be easy to determine a set of isotherm parameters that can represent all the experimental data at multiple temperatures with good accuracy. Therefore, we have used different isotherm models to fit the measured isotherm data and found that the Langmuir–Freundlich model describes the present case the best over the full range:

$$q = q_{sat}\frac{bp^{v}}{1+bp^{v}} \tag{1}$$

with T-dependent parameter b

$$b = b_0 \exp\left(\frac{E}{RT}\right) \tag{2}$$

where q, q_{sat}, p, b, and v represent the adsorbed amount, adsorption saturation capacity, pressure, equilibrium constant, and dimensionless parameter, respectively. b_0 is the value of b at infinite temperature and E is the energy change associated with adsorption. To avoid variant adsorption saturation capacity from the fitting at different temperatures, we fit the parameters (see Table 2) using the three sets of isotherms at the three different temperatures simultaneously. The fitted isotherms, shown in Fig. 2 as continuous solid lines, are in excellent agreement with the experimental data.

We observe that under the same conditions, the adsorbed amount of CO_2 on Kureha carbon is much higher than that of CH_4 or N_2. Therefore, the much higher adsorption affinity to CO_2 over CH_4 or N_2 indicates that Kureha carbon could be potentially used for the separation of CO_2/CH_4 and CO_2/N_2 mixtures.

For comparison, Table 3 also includes the isotherm data of CO_2, CH_4, and N_2 on the commercial benchmark activated carbon Maxsorb (Kansai Netsu Kagaku Co.), which has been demonstrated to possess some excellent properties for CO_2 capture [40]. On a basis of gravimetric adsorption capacity, at 298 K and 100 kPa, which are close to the post-combustion conditions for the process of CO_2 capture [31], the adsorbed amount of CO_2 on Kureha carbon is higher than that on Maxsorb while the adsorbed amounts of CH_4 and N_2 on Kureha carbon are comparable to those on Maxsorb. On the other hand, at 298 K and 2,000 kPa, which are similar to the pre-combustion conditions for CO_2 capture [31], Maxsorb has much higher adsorption capacities for these three adsorbates, compared to Kureha carbon.

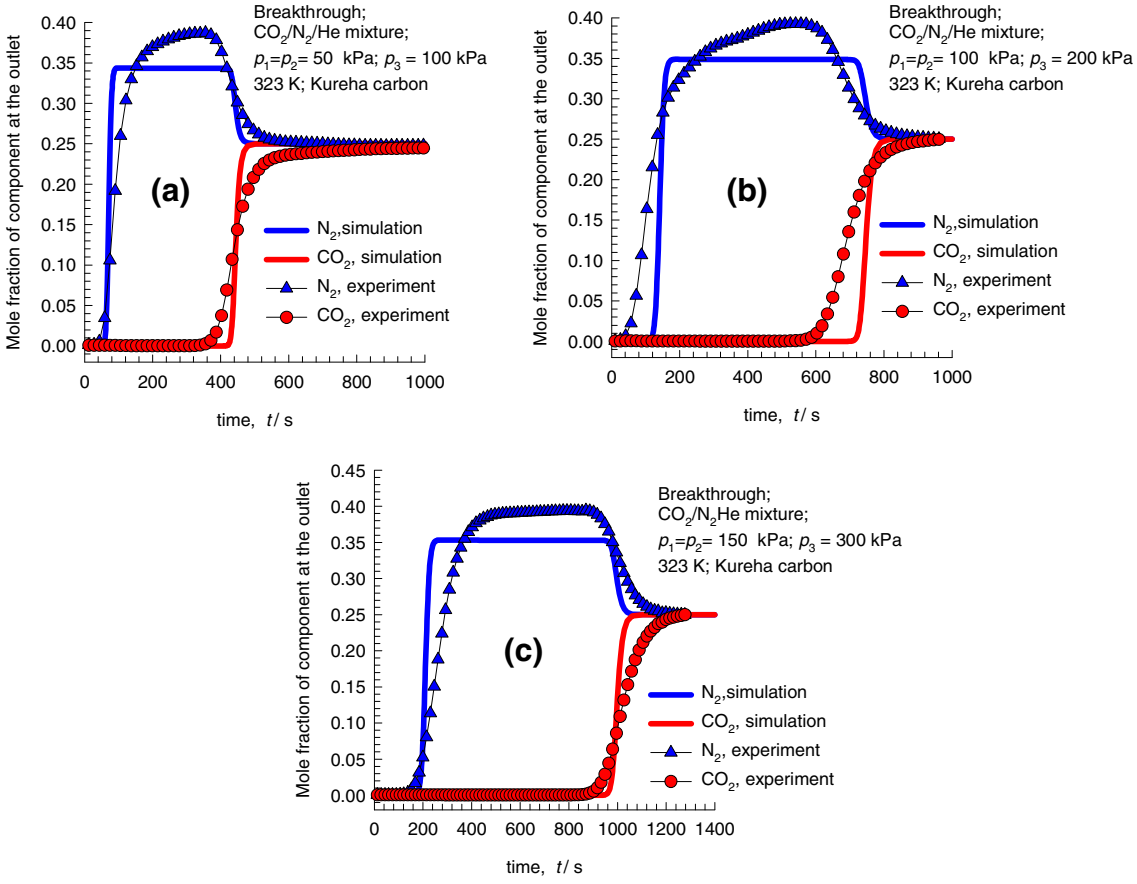

Fig. 8. Comparison of the experimental breakthroughs for $CO_2(1)/N_2(2)/He(3)$ with the corresponding breakthrough simulations at 323 K. (a) $p_1 = p_2 = 50$ kPa and $p_3 = 100$ kPa, (b) $p_1 = p_2 = 100$ kPa and $p_3 = 200$ kPa, and (c) $p_1 = p_2 = 150$ kPa and $p_3 = 300$ kPa. The continuous solid lines are the simulations assuming negligible diffusional limitations and invoking Eq. (A9).

Maxsorb has a huge surface area and pore volume, as shown in Table 1. Unlike Kureha carbon that is a purely microporous material, mesopores also contribute to the total pore volume and the surface area of Maxsorb, implying that Maxsorb has a wider pore size distribution. At the lower pressure, the adsorption process involves exclusively the smaller micropores of activated carbons. Maxima CO_2 retention capacities at the lower pressure can only be found for activated carbons with high micropore volumes coming from pores below 0.8 nm [32–35]. On the other hand, at the higher pressure, the CO_2 uptake first occurs by filling of the entire microporosity, followed by filling of the mesopores and/or macropores if available. Accordingly, the pore sizes of Kureha carbon are centered at 0.6 and 1.1 nm, respectively [36], while Maxsorb has well-developed mesopores [41]. This probably provides the reasons why Kureha carbon has a higher adsorption capacity for CO_2 at the lower pressure while Maxsorb has a higher uptake toward CO_2 at the higher pressure, at least on a gravimetric basis.

Industrial application of porous solids for CO_2 capture requires not only a high adsorption capacity on a gravimetric basis but rather a high adsorption capacity per unit volume of adsorbent. In this sense, the volumetric adsorption capacity highly depends on the final bulk density of adsorbent. Table 3 also shows the adsorption isotherm data of CO_2, CH_4, and N_2 on Kureha carbon and Maxsorb on a volumetric basis, i.e. mmol adsorbate per cm^3 of adsorbent. Considering the particle densities of the two adsorbents, the scenario changes drastically when compared to that on a gravimetric basis. Kureha carbon has a particle density of 991 kg m^{-3}, much higher than 290 kg m^{-3} for Maxsorb, see Table 1, resulting in much higher volumetric capacities for CO_2 on Kureha carbon at both lower and higher pressures. This indicates that Kureha carbon might be a better adsorbent for CO_2 capture, compared to the benchmark activated carbon Maxsorb.

3.2. Isosteric heat of adsorption

The isosteric heat of adsorption, Q_{st}, defined as

$$Q_{st} = RT^2\left(\frac{\partial \ln p}{\partial T}\right)_q \tag{3}$$

was determined using the pure component isotherm fits. The derived values of the isosteric heat of adsorption at zero loading (Q_{st}^0) for CO_2, CH_4, and N_2 on Kureha carbon are provided in Table 2, and the hierarchy of Q_{st}^0 is $CO_2 > CH_4 > N_2$, in order of the polarizability of the adsorbate, because the adsorption potential is almost entirely the product of dispersion forces, where the adsorbent-adsorbate interaction is proportional to the polarizability of the adsorbate for the nonspecific interactions involved, The derived value of Q_{st}^0 for CO_2 on Kureha carbon is within a rang from 16 to 24 kJ mol^{-1} for CO_2 on other commercial activated carbons [40], mainly related to the pore-size variety of the activated carbons.

Fig. 3 represents a comparison of the isosteric heat of adsorption of CO_2 on Kureha carbon with the data on NaX [45], MgMOF-74 [45], Cu-TDPAT [46] and NiMOF-74 [47,48] that are considered to be promising candidates for CO_2 capture. We note the Q_{st} value for Kureha carbon is significantly lower than those for the zeolite and MOFs. This implies that the cost of regeneration with Kureha carbon can be potentially lower than that of the

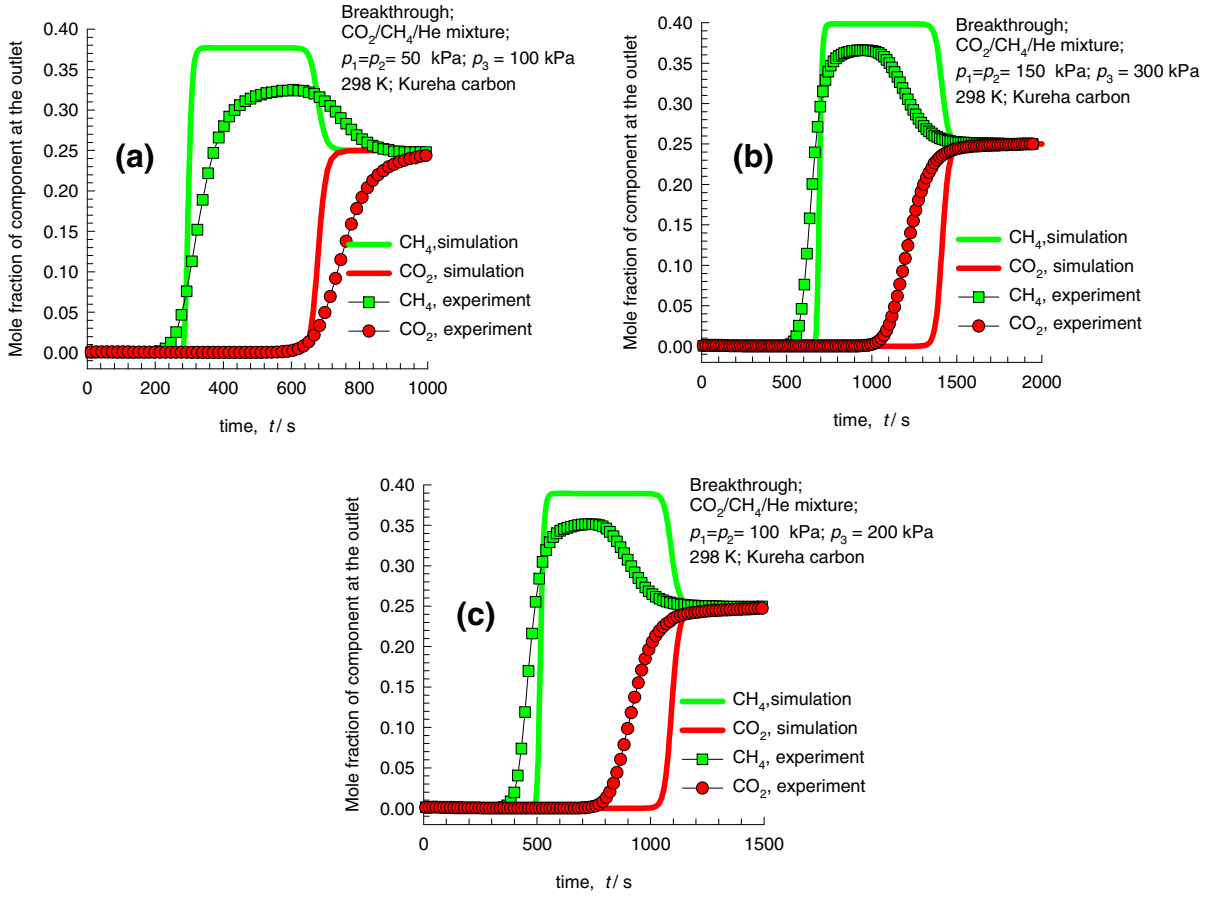

Fig. 9. Comparison of the experimental breakthroughs for $CO_2(1)/CH_4(2)/He(3)$ with the corresponding breakthrough simulations at 298 K. (a) $p_1 = p_2 = 50$ kPa and $p_3 = 100$ kPa, (b) $p_1 = p_2 = 100$ kPa and $p_3 = 200$ kPa, and (c) $p_1 = p_2 = 150$ kPa and $p_3 = 300$ kPa. The continuous solid lines are the simulations assuming negligible diffusional limitations and invoking Eq. (A9). A video animation of the transient breakthrough at 298 K and a total pressure of 200 kPa is available as Supplementary material.

representative zeolite and MOFs. This is an important advantage in favor of Kureha carbon.

3.3. IAST predictions

The selectivity of the preferential adsorption of component 1 over component 2 in a mixture containing 1 and 2, perhaps in the presence of other components too, can be formally defined as:

$$S_{ads} = \frac{q_1/q_2}{p_1/p_2} \tag{4}$$

In Eq. (4), q_1 and q_2 are the *absolute* component loadings in the adsorbed phase. These component loadings are also termed the uptake capacities. In all the calculations to be presented below, the calculations of q_1 and q_2 are based on the use of IAST by Myers and Prausnitz [49]. The algorithm used for performing the IAST calculations is summarized in our earlier work by Krishna [50]. The accuracy of the IAST calculations for estimating the component loadings for several binary mixtures in a wide variety of zeolites and MOFs has been established by comparison with Configurational-Bias Monte Carlo (CBMC) simulations of mixture adsorption [51–56].

Fig. 4 represents the adsorption selectivity as a function of total gas-phase pressure calculated by IAST for equimolar binary CO_2/CH_4 and CO_2/N_2 gas mixtures on Kureha carbon. We note that the CO_2/N_2 selectivity is significantly higher than the CO_2/CH_4 one, ascribed to the fact that the interactions between N_2 and Kureha carbon are much weaker than those between CH_4 and the adsorbent, evidenced by the isosteric heat of adsorption at zero coverage for N_2 much lower than that for CH_4, shown in Table 2. This implies that Kureha carbon could be more suitable for CO_2 capture from flue gas that typically consists of CO_2/N_2 mixtures.

Besides the adsorption selectivities, the separation performance is also dictated by the uptake capacities. Fig. 5 represents the uptake capacity of CO_2 from equimolar binary CO_2/CH_4 and CO_2/N_2 gas mixtures on Kureha carbon as a function of total gas phase pressure calculated by IAST. These results show that in both cases the uptake capacities of CO_2 are almost the same under the same conditions, implying that the presence of the second component CH_4 or N_2 hardly affects the adsorption of CO_2 due to the much stronger adsorption affinity of Kureha carbon toward CO_2.

For validation of IAST calculations, we shall compare the uptake loadings of CO_2 predicted by IAST with the values determined from the breakthrough experiments.

3.4. Transient breakthroughs

We performed the breakthrough experiments to assess the practical application of Kureha carbon in separating the gas mixtures. Figs. 6–8 represent the experimental breakthroughs for $CO_2(1)/N_2(2)/He(3)$ mixture at 298, 310, and 323 K. At each temperature the inlet partial pressures of components 1–3 were maintained as follows (a) $p_1 = p_2 = 50$ kPa and $p_3 = 100$ kPa, (b) $p_1 = p_2 = 100$ kPa and $p_3 = 200$ kPa, and (c) $p_1 = p_2 = 150$ kPa and $p_3 = 300$ kPa.

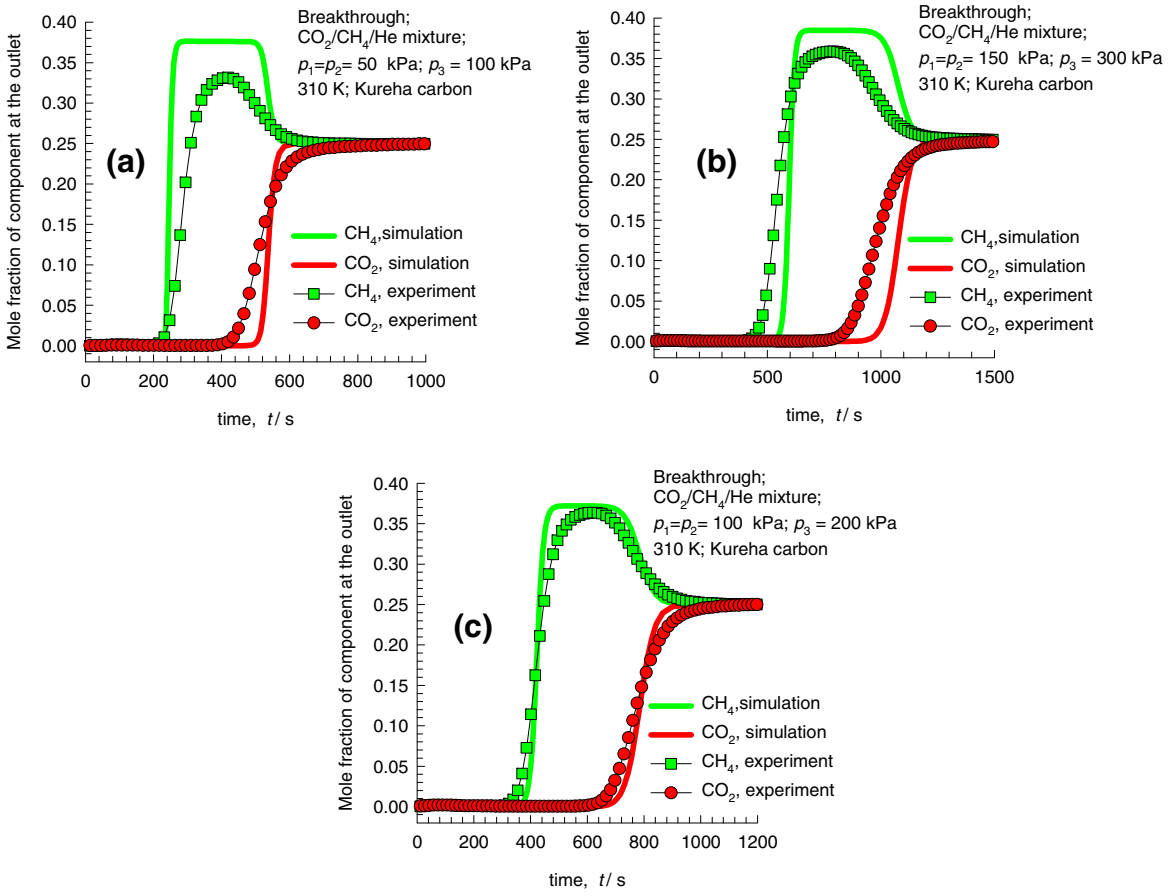

Fig. 10. Comparison of the experimental breakthroughs for $CO_2(1)/CH_4(2)/He(3)$ with the corresponding breakthrough simulations at 310 K. (a) $p_1 = p_2 = 50$ kPa and $p_3 = 100$ kPa, (b) $p_1 = p_2 = 100$ kPa and $p_3 = 200$ kPa, and (c) $p_1 = p_2 = 150$ kPa and $p_3 = 300$ kPa. The continuous solid lines are the simulations assuming negligible diffusional limitations and invoking Eq. (A9).

We are taking Fig. 6a for example to elucidate the separation performance of the $CO_2/N_2/He$ mixture through the packed bed of Kureha carbon at 298 K and a total pressure of 200 kPa. As shown in the figure, N_2 elutes through the column after 60 s and the mole fraction sharply increases to about 0.40, higher than a mole fraction of 0.33 by assuming that the gas phase only consists of N_2 and He and their flow rates are the same as those in the inlet of the column. This interesting phenomenon is ascribed to a competitive adsorption behavior between CO_2 and N_2, resulting in the replacement of the adsorbed N_2 by CO_2 due to the stronger adsorption affinity of CO_2.

Transient breakthrough simulations were then performed to model the whole process with the same conditions as those in the experiments; the details of the breakthrough simulation methodology are the same as those used in the earlier work by Krishna [50] and a summary is provided in Supplementary Material accompanying this publication. The intra-crystalline diffusion was taken into account during the breakthrough simulations that were compared to those without the consideration of the intra-particle diffusion to evaluate its effect. It is found that in both cases (i.e., with and without the consideration of the intra-particle diffusion), the simulation results are almost identical, indicating that the intra-particle diffusion could be excluded by assuming the thermodynamic equilibrium at any position in the fixed-bed adsorber during the breakthrough simulations. These simulation results are also shown by the continuous solid lines in Figs. 6–8. In all the cases, the essential characteristics of the experimental breakthroughs are well reproduced in the transient simulations. We also notice that the breakthrough times are decreased at the same total pressure as the temperature changes from 298 to 310 and 323 K, which is reasonable since the adsorption capacity of the adsorbent is lower as the temperature increases, while the breakthrough time is increased at the same temperature as the total pressure increases, ascribed to the fact that the adsorption capacity of the adsorbent is higher as the pressure increases. For each case, there is a certain period that pure N_2 elutes through the bed, suggesting that Kureha carbon adsorbent has very high separation efficiency for CO_2/N_2 mixture in this regard.

In addition to its high separation selectivity for CO_2/N_2 mixture, Kureha carbon may also be promising in separating CO_2/CH_4 mixture based on their large difference of uptakes as discussed in Section 3.1. As shown in Figs. 9–11, at all three different temperatures and pressures, CH_4 is the first to elute through the bed in a short time, whereas the solid adsorbent retains the CO_2. Take Fig. 9a for example in order to explain the differences in breakthrough between CO_2 and CH_4, CH_4 at the outlet of column sharply increases to a mole fraction of 0.33 at time = 230 s, while no CO_2 gas is detected until the time is longer than 600 s. This could be explained as the fact that the CO_2 molecules have much stronger adsorption strength on Kureha carbon than CH_4 and thus they gradually occupy all possible adsorption sites. Interestingly, the mole fraction of CH_4 is larger than 0.25 at the inlet of column in a large range of time from about 400–600 s. Two reasons may cause this roll-up effect; firstly, the CO_2 molecules are completely adsorbed on the adsorbent and thus not detected at the outlet of the column at all, and therefore the mole fraction of CH_4 could reach a value of 0.33 (1:2 CH_4/He mixture). Secondly, the CO_2 molecules may have a competing adsorption behavior over CH_4 when

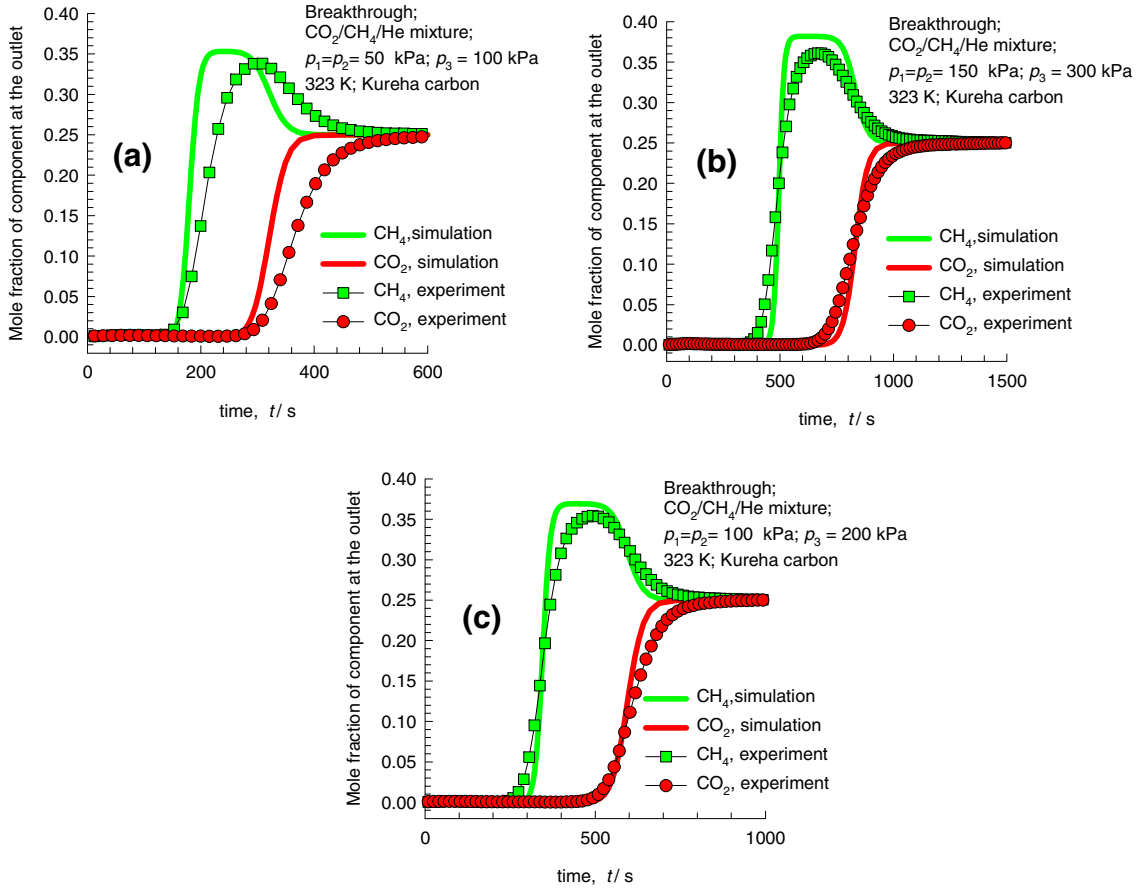

Fig. 11. Comparison of the experimental breakthroughs for $CO_2(1)/CH_4(2)/He(3)$ with the corresponding breakthrough simulations at 323 K. (a) $p_1 = p_2 = 50$ kPa and $p_3 = 100$ kPa, (b) $p_1 = p_2 = 100$ kPa and $p_3 = 200$ kPa, and (c) $p_1 = p_2 = 150$ kPa and $p_3 = 300$ kPa. The continuous solid lines are the simulations assuming negligible diffusional limitations and invoking Eq. (A9).

the available adsorption sites on Kureha carbon decrease, thus leading to an increase in the amount of CH_4 at the outlet of column.

For a quantitative comparison with the breakthrough experiments, we also carried out simulations without inclusion of intra-particle diffusion effects, see Figs. 9–11. The simulation results are in good agreement with the experimental data, especially in the cases at 323 K the agreements are excellent. The simulated breakthroughs and breakthrough experiments confirm that Kureha carbon could be also a potential candidate for separating CO_2/CH_4 mixtures.

The good agreement between experiments and simulations indicate that the separation potential of Kureha carbon is not significantly influenced by intra-particle diffusion limitations. Put another way, the separation performance is primarily dictated by adsorption equilibrium thermodynamics. This implies that the IAST calculations should provide reliable estimates of CO_2 capture capacities. We shall now attempt to seek direct verification of this conclusion.

In the breakthrough experiments, the volumetric flow of the inert gas He is maintained constant at a value Q_{He}. The experiments are carried out for a total period of time, t_{ss}, till steady-state is reached. A mass balance for the time interval $t = 0 - t_{ss}$, allows us to determine the component loadings q_i [43]:

$$(q_i - q_{i0})m_{ads} = c_t Q_{He}\int_0^{t_{ss}}\left(\frac{y_{i,inlet}}{y_{He,inlet}} - \frac{y_{i,exit}}{y_{He,exit}}\right)dt - (c_t y_{i,exit})(AL - V_{ads}) \quad (5)$$

In the adsorption phase of the breakthrough experiments, the initial loadings $q_{i0} = 0$. The second term on the right hand side represents the "dead volume correction", which is properly accounted for in our calculations. The integral in Eq. (5) can be determined numerically from the breakthrough experimental data. We used numerical quadrature formula, implemented in Excel for the calculations.

Fig. 12 represents the values of CO_2 uptakes from $CO_2(1)/N_2(2)/He(3)$ mixtures, calculated using Eq. (5) from the breakthrough experiments at 298, 310, and 323 K. These calculated CO_2 uptakes are in excellent agreement with the corresponding IAST predictions.

Although breakthrough experiments are quite valuable for evaluating the gas separation capabilities of adsorbents, in practice they can be difficult and time consuming. Assuming that (i) external mass transfer resistances and heat effects are negligible through an isothermal adsorption bed in thermodynamic equilibrium, (ii) plug flow proceeds through the bed, and (iii) the binary mixture adsorption equilibrium in the packed bed of adsorbent can be calculated using IAST, we were able to solve a set of partial differential equations and calculate breakthrough curves. Here we have demonstrated that the breakthrough characteristics could instead be simulated with reasonable accuracy. Given this validation, we can minimize breakthrough experimental work and employ analogous simulations to make quantitative comparisons with other adsorbents. However, for a large- and/or industrial-scale PSA process, the modeling or simulation should include external and/or internal mass transfer resistances, axial dispersion,

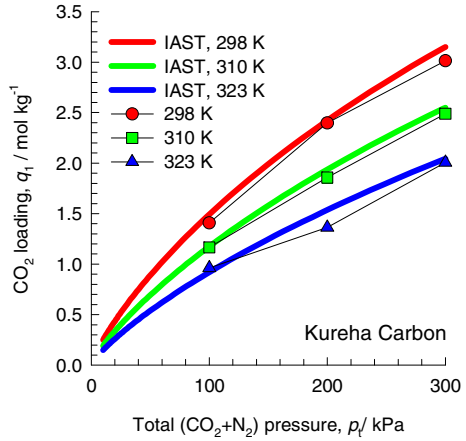

Fig. 12. Uptake capacities of CO_2 calculated from the breakthroughs of the CO_2/N_2/He mixture on Kureha carbon in comparison with the IAST predications.

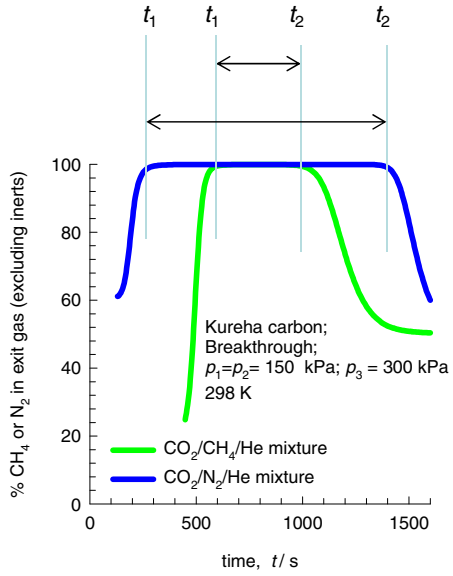

Fig. 13. Experimental breakthroughs for $CO_2(1)/CH_4(2)/He(3)$ and $CO_2(1)/N_2(2)/He(3)$ mixtures in the fixed bed packed with Kureha carbon at 298 K. The y-axis represents the $\%CH_4$ or $\%N_2$ in the exit gas stream, excluding the presence of the inert gas He. The partial pressures at the inlet are $p_1 = p_2 = 150$ kPa and $p_3 = 300$ kPa.

and heat effects. Indeed, some investigators have developed more realistic models to simulate measured single and binary breakthrough curves [57–59].

3.5. Pure gas productivities from the breakthrough experiments

As illustration, Fig. 13 compares the experimental breakthroughs for $CO_2(1)/CH_4(2)/He(3)$ and $CO_2(1)/N_2(2)/He(3)$ in the fixed bed packed with Kureha carbon at 298 K. The partial pressures at the inlet are $p_1 = p_2 = 150$ kPa and $p_3 = 300$ kPa. The y-axis represents the% CH_4 or% N_2 in the exit gas stream, excluding the presence of the inert gas He. During the time interval between t_1 and t_2, 99%+ pure CH_4 or 99%+ pure N_2 can be produced. Since the CO_2/N_2 selectivity is significantly higher than the CO_2/CH_4 one, more 99%+ pure N_2 can be produced for the same amount of Kureha carbon in the fixed bed.

A material balance for the shorter time interval $t = t_1 - t_2$, as indicated in Fig. 13, allows us to determine the productivity of CH_4 with the specified 99%+ purity:

$$\text{CH}_4 \text{ productivity} = \frac{c_t Q_{\text{He}}}{m_{ads}} \int_{t_1}^{t_2} \left(\frac{y_{\text{CH}_4,exit}}{y_{\text{He,exit}}} \right) \text{dt} \tag{6}$$

A similar material balance but for the longer time interval $t = t_1 - t_2$, as indicated in Fig. 13, can be used to determine the productivity of N_2 with the specified 99%+ purity:

$$\text{N}_2 \text{ productivity} = \frac{c_t Q_{\text{He}}}{m_{ads}} \int_{t_1}^{t_2} \left(\frac{y_{\text{N}_2,exit}}{y_{\text{He,exit}}} \right) dt \tag{7}$$

Fig. 14a represents a comparison of the productivities of 99%+ pure CH_4 for $CO_2(1)/CH_4(2)/He(3)$ breakthroughs as a function of total $(CO_2 + CH_4)$ gas pressure in the breakthrough experiments at the three different temperatures. One can see the strong influence of temperature on the productivity. Similarly, Fig. 14b represents a comparison of the productivities of 99%+ pure N_2 for $CO_2(1)/N_2(2)/He(3)$ breakthroughs as a function of total $(CO_2 + N_2)$ gas pressure in the breakthrough experiments. Under the same temperature and total gas pressure, the productivity of 99%+ pure N_2 is much higher than that of 99%+ pure CH_4.

The productivity of 99%+ pure CH_4 is expected to correlate with the CO_2 uptake capacity of Kureha carbon, which can be calculated from Eq. (6). Fig. 15a represents the plots of the productivity of 99%+ pure CH_4 versus the CO_2 uptake from $CO_2(1)/CH_4(2)/He(3)$ mixture on Kureha carbon at 298, 310 and 323 K. In all the three cases, one can see that these two parameters correlate with each other, albeit approximately in some cases. Similarly, Fig. 15b

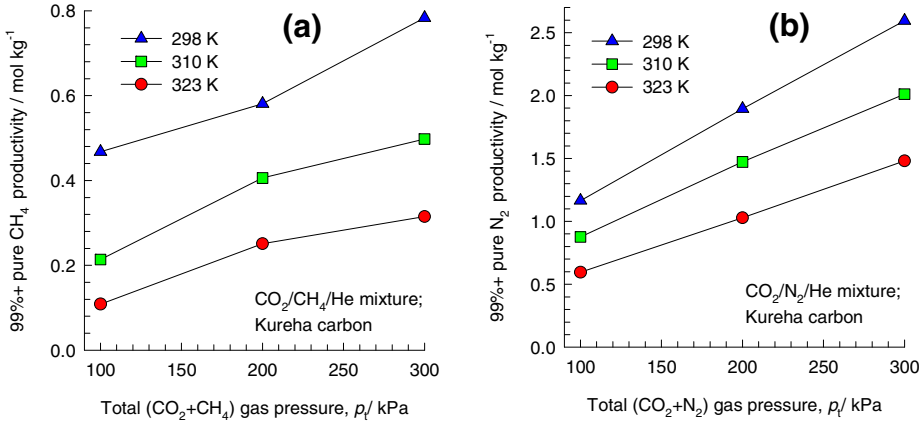

Fig. 14. Productivity of (a) 99%+ pure CH_4 for $CO_2(1)/CH_4(2)/He(3)$ and (b) 99%+ pure N_2 for $CO_2(1)/N_2(2)/He(3)$ breakthroughs as a function of total $(CO_2 + CH_4)$ or $(CO_2 + N_2)$ gas pressure.

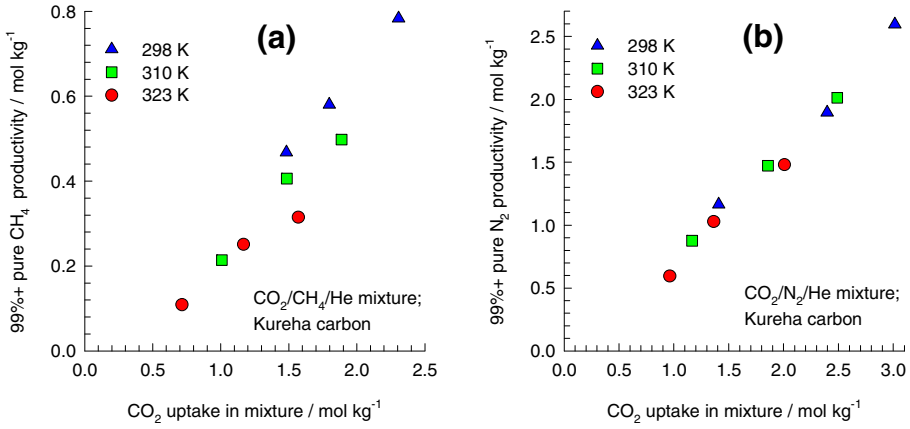

Fig. 15. Plots of the productivity of (a) 99%+ pure CH_4 and (b) 99%+ pure N_2 versus the CO_2 uptake on Kureha carbon.

represents the plots of the productivity of 99%+ pure N_2 versus the CO_2 uptake from $CO_2(1)/N_2(2)/He(3)$ mixture on Kureha carbon at the three different temperatures. These results show that higher pure gas productivities correlate with higher CO_2 uptakes, as expected.

4. Conclusions

The present study shows the potential application of Kureha carbon, which is a purely microporous material with high particle density, on selective separation of gas mixtures such as CO_2/N_2 and CO_2/CH_4. Compared to the benchmark activated carbon Maxsorb, Kureha carbon has some better properties for CO_2 capture under both post- and pre-combustion conditions, on a volumetric basis. The Langmuir–Freundlich model appropriately describes the measured equilibrium data of CO_2, CH_4, and N_2 on Kureha carbon over the whole range of conditions. The extracted isosteric heat associated with adsorption of CO_2 on Kureha carbon is significantly lower, compared to those on the zeolite and MOFs, implying that the cost of regeneration with Kureha carbon can be potentially lower. To evaluate its practical applications we focus on studying the separation efficiency via breakthrough experiments as well as breakthrough simulations proposed recently, which have been proven to be a realistic tool for screening adsorbents for separations. The breakthrough results show that Kureha carbon exhibits a high selectivity for CO_2 over N_2 and CH_4, thus capturing pure CO_2 from CO_2/N_2 and CO_2/CH_4 mixtures, respectively, under certain conditions. The simulations agree reasonably well with the experiments for all the mixtures investigated in this study, showing that the separation performance is not significantly influenced by the intra-particle diffusion resistances and the IAST calculations are found to satisfactorily predict the experimentally observed separation performance. The results indicate that Kureha carbon has a significant potential for CO_2 uptake from flue gas mixtures.

Acknowledgements

W.Z. and D.C. gratefully acknowledge the support from the National Natural Science Foundation of China (21036006, 21303165, and 21476214).

Appendix A. Supplementary data

Simulation methodology for transient breakthroughs, data file of the experimental breakthroughs in Excel, and two video animations of the transient breakthroughs of $CO_2(1)/N_2(2)/He(3)$ and $CO_2(1)/CH_4(2)/He(3)$ with $p_1 = p_2 = 50$ kPa and $p_3 = 100$ kPa at 298 K. These supplementary data associated with this article can be found in the online version at doi: http://dx.doi.org/10.1016/j.cej.2015.01.091.

References

[1] R. Quadrelli, S. Peterson, The energy–climate challenge: recent trends in CO_2 emissions from fuel combustion, Energy Policy 35 (2007) 5938–5952.
[2] R.K. Pachauri, A. Reisinger, 27th Session of the Intergovernmental Panel on Climate Change: Fourth Assessment Report, Valencia, Spain, 2007.
[3] K. Sumida, D.L. Rogow, J.A. Mason, J.M. McDonald, E.D. Bloch, Z.R. Herm, T.H. Bae, J.R. Long, Carbon dioxide capture in metal–organic frameworks, Chem. Rev. 112 (2012) 724–781.
[4] H. Yang, Z.H. Xu, M.H. Fan, R. Gupta, R.B. Slimane, A.E. Bland, I. Wright, Progress in carbon dioxide separation and capture: a review, J. Environ. Sci. 20 (2008) 14–27.
[5] S. Harimurti, B. Dutta, I. Ariff, S. Chakrabarti, D. Vione, Degradation of monoethanolamine in aqueous solution by fenton's reagent with biological post-treatment, Water Air Soil Pollut. 211 (2010) 273–286.
[6] X.L. Ma, X.X. Wang, C.S. Song, "Molecular basket" sorbents for separation of CO_2 and H_2S from various gas streams, J. Am. Chem. Soc. 131 (2009) 5777–5783.
[7] S.Y. Hao, H. Chang, Q. Xiao, Y.J. Zhong, W.D. Zhu, One-pot synthesis and CO_2 adsorption properties of ordered mesoporous SBA-15 materials functionalized with APTMS, J. Phys. Chem. C 115 (2011) 12873–12882.
[8] Y. Wang, M.D. LeVan, Adsorption equilibrium of carbon dioxide and water vapor on zeolites 5A and 13X and silica gel: pure components, J. Chem. Eng. Data 54 (2009) 2839–2844.
[9] J. Jiang, J. Yu, A. Corma, Extra-large-pore zeolites: bridging the gap between micro and mesoporous structures, Angew. Chem. Int. Ed. 49 (2010) 3120–3145.
[10] M. Palomino, A. Corma, F. Rey, S. Valencia, New insights on CO_2–methane separation using LTA zeolites with different Si/Al ratios and a first comparison with MOFs, Langmuir 26 (2010) 1910–1917.
[11] J. Zhang, P.A. Webley, P. Xiao, Effect of process parameters on power requirements of vacuum swing adsorption technology for CO_2 capture from flue gas, Energy Convers. Manage. 49 (2008) 346–356.
[12] G. Li, P. Xiao, P. Webley, J. Zhang, R. Singh, M. Marshall, Capture of CO_2 from high humidity flue gas by vacuum swing adsorption with zeolite 13X, Adsorption 14 (2008) 415–422.
[13] G. Li, P. Xiao, P. Webley, J. Zhang, R. Singh, Competition of CO_2/H_2O in adsorption based CO_2 capture, Energy Procedia 1 (2009) 1123–1130.
[14] N. Konduru, P. Linder, N.M. Assaf-Anid, Curbing the greenhouse effect by carbon dioxide adsorption with zeolite 13X, AIChE J. 53 (2007) 3137–3143.
[15] W.D. Zhu, P. Hrabanek, L. Gora, F. Kapteijn, J.A. Moulijn, Role of adsorption in the permeation of CH_4 and CO_2 through a silicalite-1 membrane, Ind. Eng. Chem. Res. 45 (2006) 767–776.
[16] J. van den Bergh, W.D. Zhu, F. Kapteijn, J. Gascon, J.A. Moulijn, Separation and permeation characteristics of a DD3R zeolite membrane, J. Membr. Sci. 316 (2008) 35–45.
[17] J.R. Li, J. Sculley, H.C. Zhou, Metal–organic frameworks for separations, Chem. Rev. 112 (2012) 869–932.
[18] J. Liu, P.K. Thallapally, B.P. McGrail, D.R. Brown, J. Liu, Progress in adsorption-based CO_2 capture by metal–organic frameworks, Chem. Soc. Rev. 41 (2012) 2308–2322.
[19] P.L. Llewellyn, S. Bourrelly, C. Serre, A. Vimont, M. Daturi, L. Hamon, G.D. Weireld, J.S. Chang, D.Y. Hong, Y.K. Hwang, S.H. Jhung, G. Ferey, High uptakes

of CO_2 and CH_4 in mesoporous metal-organic frameworks MIL-100 and MIL-101, Langmuir 24 (2008) 7245–7250.
[20] O.K. Farha, A.O. Yazaydn, I. Eryazici, C.D. Malliakas, B.G. Hauser, M.G. Kanatzidis, S.T. Nguyen, R.Q. Snurr, J.T. Hupp, De novo synthesis of a metal–organic framework material featuring ultrahigh surface area and gas storage capacities, Nat. Chem. 2 (2010) 944–948.
[21] H. Furukawa, N. Ko, Y.B. Go, N. Aratani, S.B. Choi, E. Choi, A.O. Yazaydinet, R.Q. Snurr, M. O'Keeffe, J. Kim, O.M. Yaghi, Ultrahigh porosity in metal–organic frameworks, Science 329 (2010) 424–428.
[22] D. Wu, Q. Xu, D.H. Liu, C.L. Zhong, Exceptional CO_2 capture capability and molecular-level segregation in a Li-modified metal–organic framework, J. Phys. Chem. C 114 (2010) 16611–16617.
[23] Q. Xu, D.H. Liu, Q.Y. Yang, C.L. Zhong, J.G. Mi, Li-modified metal–organic frameworks for CO_2/CH_4 separation: a route to achieving high adsorption selectivity, J. Mater. Chem. 20 (2010) 706–714.
[24] L. Bastin, P.S. Barcia, E.J. Hurtado, J.A.C. Silva, A.E. Rodrigues, B. Chen, A microporous metal–organic framework for separation of CO_2/N_2 and CO_2/CH_4 by fixed-bed adsorption, J. Phys. Chem. C 112 (2007) 1575–1581.
[25] A. Phan, C.J. Doonan, F.J. Uribe-Romo, C.B. Knobler, M. O'Keeffe, O.M. Yaghi, Synthesis, structure, and carbon dioxide capture properties of zeolitic imidazolate frameworks, Acc. Chem. Res. 43 (2010) 58–67.
[26] A.C. Kizzie, A.G. Wong-Foy, A.J. Matzger, Effect of humidity on the performance of microporous coordination polymers as adsorbents for CO_2 capture, Langmuir 27 (2011) 6368–6373.
[27] J. Liu, Y. Wang, A.I. Benin, P. Jakubczak, R.R. Willis, M.D. LeVan, CO_2/H_2O adsorption equilibrium and rates on metal–organic frameworks: HKUST-1 and Ni/DOBDC, Langmuir 26 (2010) 14301–14307.
[28] S. Choi, J.H. Drese, C.W. Jones, Adsorbent materials for carbon dioxide capture from large anthropogenic point sources, ChemSusChem 2 (2009) 796–854.
[29] M.G. Plaza, S. García, F. Rubiera, J.J. Pis, C. Pevida, Post-combustion CO_2 capture with a commercial activated carbon: comparison of different regeneration strategies, Chem. Eng. J. 163 (2010) 41–47.
[30] D.P. Valenzuela, A.L. Myers, Adsorption Equilibrium Data Handbook, Prentice Hall, New Jersey, 1989.
[31] C.F. Martin, M.G. Plaza, J.J. Pis, F. Rubiera, C. Pevida, T.A. Centeno, On the limits of CO_2 capture capacity of carbons, Sep. Purif. Technol. 74 (2010) 225–229.
[32] M. Sevilla, J.B. Parra, A.B. Fuertes, Assessment of the role of micropore size and N-doping in CO_2 capture by porous carbons, ACS Appl. Mater. Interfaces 5 (2013) 6360–6368.
[33] M. Sevilla, C. Falco, M.-M. Titirici, A.B. Fuertes, High-performance CO_2 sorbents from algae, RSC Adv. 2 (2012) 12792–12797.
[34] V. Presser, J. McDonough, S.-H. Yeon, Y. Gogotsi, Effect of pore size on carbon dioxide sorption by carbide derived carbon, Energy Environ. Sci. 4 (2011) 3059–3066.
[35] H. Wei, S. Deng, B. Hu, Z. Chen, B. Wang, J. Huang, G. Yu, Granular bamboo-derived activated carbon for high CO_2 adsorption: the dominant role of narrow micropores, ChemSusChem 5 (2012) 2354–2360.
[36] W.D. Zhu, J.C. Groen, F. Kapteijn, J.A. Moulijn, Adsorption of butane isomers and SF_6 on Kureha activated carbon: 1. Equilibrium, Langmuir 20 (2004) 5277–5284.
[37] W.D. Zhu, F. Kapteijn, J.C. Groen, M.J.G. Linders, J.A. Moulijn, Adsorption of butane isomers and SF_6 on Kureha activated carbon: 2. Kinetics, Langmuir 20 (2004) 1704–1710.
[38] W.D. Zhu, J.C. Groen, A. van Miltenburg, F. Kapteijn, J.A. Moulijn, Comparison of adsorption behaviour of light alkanes and alkenes on Kureha activated carbon, Carbon 43 (2005) 1416–1423.
[39] W.D. Zhu, F. Kapteijn, J.C. Groen, J.A. Moulijn, Adsorption on Kureha activated carbon: isotherms and kinetics, Adsorption 11 (2005) 637–641.
[40] S. Himeno, T. Komatsu, S. Fujita, High-pressure adsorption equilibria of methane and carbon dioxide on several activated carbons, J. Chem. Eng. Data 50 (2005) 369–376.
[41] W. Xing, S.Z. Qiao, R.G. Ding, F. Li, G.Q. Lu, Z.F. Yan, H.M. Cheng, Superior electric double layer capacitors using ordered mesoporous carbons, Carbon 44 (2006) 216–244.
[42] D.L. Chen, H. Shang, W.D. Zhu, R. Krishna, Transient breakthroughs of CO_2/CH_4 and C_3H_6/C_3H_8 mixtures in fixed beds packed with Ni-MOF-74, Chem. Eng. Sci. 117 (2014) 407–415.
[43] D.L. Chen, N.W. Wang, F.F. Wang, J.W. Xie, Y.J. Zhong, W.D. Zhu, J.K. Johnson, R. Krishna, Utilizing the gate-opening mechanism in ZIF-7 for adsorption discrimination between N_2O and CO_2, J. Phys. Chem. C 118 (2014) 17831–17837.
[44] M.A. Sheikh, M.M. Hassan, K.F. Laughlin, Adsorption equilibria and rate parameters for nitrogen and methane on Maxsorb activated carbon, Gas Sep. Purif. 10 (1996) 161–168.
[45] J.A. Mason, K. Sumida, Z.R. Herm, R. Krishna, J.R. Long, Evaluating metal–organic frameworks for post-combustion carbon dioxide capture via temperature swing adsorption, Energy Environ. Sci. 4 (2011) 3030–3040.
[46] H. Wu, K. Yao, Y. Zhu, B. Li, Z. Shi, R. Krishna, J. Li, Cu-TDPAT, an rht-type dual-functional metal–organic framework offering significant potential for use in H_2 and natural gas purification processes operating at high pressures, J. Phys. Chem. C 116 (2012) 16609–16618.
[47] R. Krishna, J.M. van Baten, Investigating the relative influences of molecular dimensions and binding energies on diffusivities of guest species inside nanoporous crystalline materials, J. Phys. Chem. C 116 (2012) 23556–23568.
[48] R. Krishna, J.M. van Baten, Investigating the influence of diffusional coupling on mixture permeation across porous membranes, J. Membr. Sci. 430 (2013) 113–128.
[49] A.L. Myers, J.M. Prausnitz, Thermodynamics of mixed gas adsorption, AIChE J. 11 (1965) 121–130.
[50] R. Krishna, The Maxwell–Stefan description of mixture diffusion in nanoporous crystalline materials, Microporous Mesoporous Mater. 185 (2014) 30–50.
[51] R. Krishna, J.M. van Baten, Using molecular simulations for screening of zeolites for separation of CO_2/CH_4 mixtures, Chem. Eng. J. 133 (2007) 121–131.
[52] R. Krishna, J.M. van Baten, In silico screening of zeolite membranes for CO_2 capture, J. Membr. Sci. 360 (2010) 323–333.
[53] R. Krishna, J.M. van Baten, In silico screening of metal-organic frameworks in separation applications, Phys. Chem. Chem. Phys. 13 (2011) 10593–10616.
[54] R. Krishna, J.M. van Baten, Maxwell–Stefan modeling of slowing-down effects in mixed gas permeation across porous membranes, J. Membr. Sci. 383 (2011) 289–300.
[55] R. Krishna, J.M. van Baten, Investigating the potential of MgMOF-74 membranes for CO_2 capture, J. Membr. Sci. 377 (2011) 249–260.
[56] R. Krishna, J.M. van Baten, Investigating the validity of the Bosanquet formula for estimation of diffusivities in mesopores, Chem. Eng. Sci. 69 (2012) 684–688.
[57] C. Shen, C.A. Grande, P. Li, J. Yu, A.E. Rodrigues, Adsorption equilibria and kinetics of CO_2 and N_2 on activated carbon beads, Chem. Eng. J. 160 (2010) 398–407.
[58] A.F.P. Ferreira, A. Mafalda Ribeiro, S. Kulaç, A.E. Rodrigues, Methane purification by adsorptive processes on MIL-53(Al), Chem. Eng. Sci., in press (http://dx.doi.org/10.1016/j.ces.2014.06.014).
[59] F. Montagnaro, A. Silvestre-Albero, J. Silvestre-Albero, F. Rodríguez-Reinoso, A. Erto, A. Lancia, M. Balsamo, Post-combustion CO_2 adsorption on activated carbons with different textural properties, Microporous Mesoporous Mater., in press (http://dx.doi.org/10.1016/j.micromeso.2014.09.037).

Supplementary material

Utilizing transient breakthroughs for evaluating the potential of Kureha carbon for CO_2 capture

Hui Yu[a], Xue Wang[a], Chunhui Xu[a], De-Li Chen[a], Weidong Zhu[a,*], Rajamani Krishna[b,*]

[a]*Key Laboratory of the Ministry of Education for Advanced Catalysis Materials, Institute of Physical Chemistry, Zhejiang Normal University, 321004 Jinhua, P. R. of China*

[b]*Van't Hoff Institute for Molecular Science, University of Amsterdam, Science Park 904, 1098 XH Amsterdam, The Netherlands*

*Corresponding authors. Tel: +86 579 82282932. E-mail: weidongzhu@zjnu.cn (W. Zhu); E-mail: r.krishna@contact.uva.nl (R. Krishna)

Simulation methodology for transient breakthroughs

The mixture separation is commonly carried out in fixed-bed adsorbers, in which the separation performance is dictated by a combination of three separate factors: (a) adsorption selectivity, (b) uptake capacity, and (c) intra-particle diffusivities of guest molecules within the pores of adsorbent.

The simulation methodology used in this work is described in earlier publications [1-4]. A brief summary of the simulation methodology is provided below.

Assuming plug flow of an *n*-component gas mixture through a fixed bed maintained under isothermal conditions, the partial pressures in the gas phase at any position and instant of time are obtained by solving the following set of partial differential equations for each of the species *i* in the gas mixture [5].

$$\frac{1}{RT}\frac{\partial p_i(t,z)}{\partial t} = -\frac{1}{RT}\frac{\partial\left(v(t,z)\,p_i(t,z)\right)}{\partial z} - \frac{\left(1-\varepsilon\right)}{\varepsilon}\rho\frac{\partial \bar{q}_i(t,z)}{\partial t}; \quad i = 1,2,...n \tag{A1}$$

In Eq. (A1), t is the time, z is the distance along the adsorber, ρ is the particle density of adsorbent, ε is the bed voidage, v is the interstitial gas velocity, and $\bar{q}_i(t,z)$ is the *spatially averaged* molar loading within the particle with radius r_c, monitored at position z and at time t.

At any time t, during the transient approach to thermodynamic equilibrium, the spatially averaged molar loading within the particle with radius r_c is obtained by integration of the radial loading profile.

$$\bar{q}_i(t) = \frac{3}{r_c^3}\int_0^{r_c} q_i(r,t)r^2 dr \tag{A2}$$

For transient unary uptake within a particle at any position and time in a fixed bed, the radial distribution of molar loadings, q_i, within a spherical particle with radius r_c, is obtained from a solution of a set of differential equations describing the uptake:

$$\frac{\partial q_i(r,t)}{\partial t} = -\frac{1}{\rho}\frac{1}{r^2}\frac{\partial}{\partial r}\left(r^2 N_i\right) \tag{A3}$$

The molar flux N_i of component i is described by the simplified version of the Maxwell-Stefan equations, in which both correlation effects and thermodynamic coupling effects are considered to be of negligible importance [4].

$$N_i = -\rho Đ_i \frac{\partial q_i}{\partial r} \tag{A4}$$

Summing Eq. (A2) over all n species in the mixture allows calculation of the *total average* molar loading of the mixture within the particles:

$$\bar{q}_t(t,z) = \sum_{i=1}^{n} \bar{q}_i(t,z) \tag{A5}$$

The *interstitial* gas velocity is related to the *superficial* gas velocity (u) by

$$v = \frac{u}{\varepsilon} \tag{A6}$$

In industrial practice, the most common operation uses a step-wise input of mixtures to be separated into an adsorber bed that is initially free of adsorbates, i.e. we have the initial conditions:

$$t = 0; \quad q_i(0,z) = 0 \tag{A7}$$

At time, $t = 0$, the inlet to the adsorber, $z = 0$, is subjected to a step input of an n-component gas mixture and this step input is maintained till the end of the adsorption cycle when steady-state conditions are reached.

$$t \geq 0; \quad p_i(0,t) = p_{i0}; \quad u(0,t) = u \tag{A8}$$

where u is the superficial gas velocity at the inlet to the adsorber.

The breakthrough characteristics for any component are essentially dictated by two sets of parameters: (a) The characteristic contact time $\frac{L}{v} = \frac{L\varepsilon}{u}$ between the particles and the surrounding

fluid phase and (b) $\frac{Đ_i}{r_c^2}$ that reflects the importance of intra-particle diffusion limitations. It is common to use the dimensionless time, $\tau = \frac{tu}{L\varepsilon}$, obtained by dividing the actual time, t, by the characteristic time, $\frac{L\varepsilon}{u}$, when plotting simulated breakthrough curves [3].

If the value of $\frac{Đ_i}{r_c^2}$ is large enough to ensure that intra-particle gradients are absent and the entire particle can be considered to be in thermodynamic equilibrium with the surrounding bulk gas phase at that time t, and position z of the adsorber.

$$\bar{q}_i(t,z) = q_i(t,z) \tag{A9}$$

The molar loadings at the *outer surface* of the particles, i.e. at $r = r_c$, are calculated on the basis of adsorption equilibrium with the bulk gas phase partial pressures p_i at that position z and time t. The adsorption equilibrium can be calculated on the basis of the ideal adsorbed solution theory (IAST). The assumption of thermodynamic equilibrium at every position z and any time t, i.e. invoking Eq. (A9), generally results in sharp breakthroughs for each component. Sharp breakthroughs are desirable in practice because this would result in high productivity of pure products. Essentially, the influence of intra-particle diffusion is to reduce the productivity of pure gases. For all the breakthrough calculations reported in this work, we assume negligible diffusion resistances for all guest molecules and we invoke the simplified Eq. (A9).

Nomenclature

$Đ_i$ Maxwell-Stefan diffusivity, $m^2\ s^{-1}$

L length of the packed bed adsorber, m

n number of species in the mixture, dimensionless

N_i molar flux of species i, mol $m^{-2}\ s^{-1}$

p_i partial pressure of species i in the mixture, Pa

q_i component molar loading of species *i*, mol kg^{-1}

$\bar{q}_i$ average component molar loading of species *i*, mol kg^{-1}

$\bar{q}_t$ total average molar loading of the mixture, mol kg^{-1}

R universal gas law constant, 8.314 J mol^{-1} K^{-1}

r_c radius of adsorbent particle, m

t time, s

T temperature, K

u superficial gas velocity in the packed bed, m s^{-1}

v interstitial gas velocity in the packed bed, m s^{-1}

z distance along the adsorber, m

Greek letters

ε voidage of the packed bed, dimensionless

ρ particle density of adsorbent, kg m^{-3}

References

[1] D.L. Chen, H. Shang, W.D. Zhu, R. Krishna, Transient breakthroughs of CO_2/CH_4 and C_3H_6/C_3H_8 mixtures in fixed beds packed with Ni-MOF-74, Chem. Eng. Sci. 117 (2014) 407–415.

[2] D.L. Chen, N.W. Wang, F.F. Wang, J.W. Xie, Y.J. Zhong, W.D. Zhu, J.K. Johnson, R. Krishna, Utilizing the gate-opening mechanism in ZIF‑7 for adsorption discrimination between N_2O and CO_2, J. Phys. Chem. C 118 (2014) 17831–17837.

[3] R. Krishna, J.R. Long, Screening metal-organic frameworks by analysis of transient breakthrough of gas mixtures in a fixed bed adsorber, J. Phys. Chem. C 115 （2011） 12941–12950.

[4] R. Krishna, The Maxwell-Stefan description of mixture diffusion in nanoporous crystalline

materials, Microporous Mesoporous Mater. 185 (2014) 30–50.

[5] R. Krishna, R. Baur, Modelling issues in zeolite based separation processes, Sep. Purif. Technol. 33 (2003) 213–254.